

On an improved radar imaging theory of marine sand wave signatures applicable to TerraSAR-X data

I. Hennings & D. Herbers

Leibniz-Institut für Meereswissenschaften an der Universität Kiel (IFM-GEOMAR), Kiel, Germany

ABSTRACT: An improved radar imaging theory of marine sand wave signatures based on quasi-specular scattering is presented. For quasi-specular scattering from a rough ocean surface, the normalized radar cross section (NRCS) is proportional to the total variance of slopes created by ocean surface waves. Quasi-specular scattering becomes dominant at higher radar frequencies. The formulated theory is applicable to the X-band synthetic aperture radar (SAR) of TerraSAR-X, Germany's first civil national remote sensing satellite realized by a public-private partnership. The improved quasi-scattering theory contains the additional dependences on the up- and crosswind wave slopes, the angle between the upwind and perpendicular current direction to the sand wave crest, and the angle between the radar range direction and the upwind direction. The current-short surface wave interaction is described by weak hydrodynamic interaction theory in the relaxation time approximation. Due to the high spatial resolution of the TerraSAR-X data it will be possible to identify sea surface roughness variations caused by meso-scale sand waves < 300 m widths at water depths < 40 m and associated unique oceanographic phenomena such as up- and downwelling events, turbulence, and eddies.

1. INTRODUCTION

Predicted climate change and related sea-level rise will strongly modify hydro-, sediment- and morphodynamics in coastal zones worldwide. Parts of the seabed in the North Sea belong to such marine areas in the world which have been very densely sampled. One of the most striking sites with different seabed features is the extensive sand wave field in the southern North Sea. The exploration of the sea floor of the Dutch sector in the North Sea for sand and gravel resources, seabed morphology and dynamics has been recently summarized by Laban (2006). Sand transport influenced by ocean waves, currents and tides are complex processes. Therefore, research is required on the sources, properties and transport budgets of terrestrial and marine sediments in coastal areas. Basic research is necessary to achieve new insights into wave- and current-induced sand transport over sea beds covered by bedforms such as sand waves. These investigations are important for assimilation of predictive coastal morphological models.

It turned out during the last two decades that the wavy sea bed - water current - sea surface - radar backscatter interaction mechanism is also a rather complex process. However, radar remote sensing techniques has become operationally during the last three decades and has now been established among

other observation tools in marine earth sciences. Radar signatures of sea bottom topography are dominated by Bragg scattering since most of the imaging radars operate at incidence angles between 20° and 70° (Valenzuela 1978). At low radar incidence angles, < 20°, quasi-specular scattering is dominating. In addition, quasi-specular scattering becomes dominant at higher radar frequencies. According to Bragg scattering theory, the normalized radar cross section (NRCS) for small water surface waves is proportional to the wave height spectral density at the Bragg backscatter wavenumbers. For quasi-specular scattering from a rough ocean surface, the NRCS is proportional to the total variance of slopes created by ocean surface waves. The radar imaging mechanism of sea bottom topography depends strongly on radar incidence angle, radar frequency, radar polarization, current speed and -direction, as well as wind speed and -direction. The most important assumption for the radar imaging mechanism of submarine bedforms is the presence of strong currents, preferably tidal currents $\geq 0.5 \text{ m s}^{-1}$ at wind speeds $\leq 8 \text{ m s}^{-1}$. The mathematical formulation of the radar imaging mechanism of the sea bed as well as experimentally studies of these phenomena are subjects of several past and present international research activities (Alpers & Hennings 1984, Phillips 1984, Shuchman et al. 1985, Zimmerman 1985, Holliday et al. 1986, Van Gastell 1987, Romeiser & Alpers 1997, Vogel-

zang 1997, Inglada & Garello 2002, Lamont-Smith et al. 2005, Hennings & Herbers 2006, Marghany & Hashim 2006).

It is commonly known that L- and P-band imaging radar systems are to be most suitable to show radar signatures of the sea bed. On the other hand, data of spaceborne X-band synthetic aperture radar (SAR) systems have been not analysed sufficiently enough within the scientific community. To get more experiences also of this frequency band in the microwave part of the electromagnetic spectrum for the radar imaging of the ocean surface showing sea bottom topography signatures it is important to analyse X-band data systematically too.

New in situ measurements show up- and downwelling phenomena of the three-dimensional current velocity field contributing significantly to the interaction between marine sand waves and the tidal flow, which has not been known before in detail (Hennings et al. 2004). Similar circulation patterns associated with Langmuir supercells off the coast of New Jersey of the eastern USA coast have been identified also by Gargett et al. (2004). The up- and downwelling regimes cause remarkable depressions at the troughs of sand waves with a maximum depth of 2 m and a width of up to 50 m. These depressions are superimposed with current ripples which are oriented perpendicular to the dominant tidal current direction. It is expected that at the depressions of the sea bed so-called waterspouts will be created by the upward orientated component of the three-dimensional current velocity field generating turbulence patterns or boils at the water surface. It is supposed that within the boils enhanced sediment concentration or other water constituents can be observed. Consequently, it is assumed that waterspouts and boils are an additional mechanism for sediment transport in tidal channels and similar shallow environments. They may be also a major trigger of biogeochemical as well as physical processes of shallow seas. The theoretical work of these observations, processes, and interactions is still under development for complete mathematical solutions.

The improved quasi-specular scattering theory is described in the first section. The TerraSAR-X high resolution spotlight mode, the proposed measurement configuration and the selected study area are briefly presented in the second and third sections, respectively. Finally, the last section contains the conclusions.

2. THEORY

The NRCS σ_0 for finitely conductive rough surfaces based on quasi-specular scattering is given by Barrick (1968)

$$\sigma_0(\theta_0) = \pi |R(0)|^2 \sec^4 \theta_0 p_0(\zeta_{x_0}, \zeta_{y_0}) \quad (1)$$

where $R(0)$ is the Fresnel reflection coefficient at normal incidence, θ_0 is the angle of incidence, $p_0(\zeta_{x_0}, \zeta_{y_0})$ is the background joint-probability density of slopes of the vertical elevation of the sea surface ζ_0 , $\zeta_{x_0} = \partial \zeta_0 / \partial x$ and $\zeta_{y_0} = \partial \zeta_0 / \partial y$ are the slopes of the rough sea surface in two orthogonal directions, x and y . For an isotropic rough ocean surface obeying Gaussian statistics according to the incident angle dependence for quasi-specular scattering equation (1) is rewritten as

$$\sigma_0(\theta_0) = \pi \frac{|R(0)|^2}{s_0^2} \sec^4 \theta_0 \exp\left(-\frac{\tan^2 \theta_0}{s_0^2}\right) \quad (2)$$

where s_0^2 is the total variance of slopes created by the ocean waves. Relation (2) has been used as a first-order theory by Hennings & Herbers (2006) for simulations of the NRCS modulation due to quasi-specular scattering at very low grazing angle illumination caused by marine sand waves.

At short radar wavelengths, the probability density distribution function for sea surface slopes published by Cox & Munk (1954) will be used here. It has been shown by Cox & Munk (1954) that the probability density distribution of surface wave slopes, $p_0(\zeta_{x_0}, \zeta_{y_0})$ (see equation (1)), is a Gram-Charlier series (Trueblood et al. 1996) with a variance of wave slopes depending on wind speed and direction. This distribution can be expressed as

$$\begin{aligned} p_0(\zeta_{x_0}, \zeta_{y_0}) \approx & \frac{1}{2\pi \sigma_{u_0} \sigma_{c_0}} \times \\ & \left\{ \exp\left[-\frac{1}{2}(s_{u_0}^2 + s_{c_0}^2)\right] \right\} \times \\ & \left\{ 1 - \left(\frac{1}{2}\right) c_{21}(s_{c_0}^2 - 1) - \right. \\ & \left. \left(\frac{1}{6}\right) c_{03}(s_{u_0}^3 - 3s_{u_0}) + \right. \\ & \left. \left(\frac{1}{4}\right) c_{22}(s_{c_0}^2 - 1)(s_{u_0}^2 - 1) + \right. \\ & \left. \left(\frac{1}{24}\right) [c_{40}(s_{c_0}^4 - 6s_{c_0}^2 + 3) + \right. \\ & \left. c_{04}(s_{u_0}^4 - 6s_{u_0}^2 + 3)] \right\} \quad (3) \end{aligned}$$

where the leading term on the right hand side of expression (3) represents a Gaussian distribution as shown above by equation (2). This proposed improved quasi-scattering theory contains the additional influence of the up- and crosswind wave

slopes, the angle between the upwind and perpendicular current direction to the sand wave crest, and the angle between the radar range direction and the upwind direction. The squared normalized background upwind and crosswind slope are defined as

$$s_{u_0}^2 = \frac{\zeta_{x_0}^2}{\sigma_{u_0}^2} \quad (4a)$$

and

$$s_{c_0}^2 = \frac{\zeta_{y_0}^2}{\sigma_{c_0}^2} \quad (4b)$$

The variances of the background upwind and crosswind slopes are given by

$$\sigma_{u_0}^2 = a + bu_w \quad (5a)$$

and

$$\sigma_{c_0}^2 = c + du_w \quad (5b)$$

where u_w is the wind speed.

The skewness coefficients are expressed by

$$c_{21} = e - fu_w \quad (6a)$$

and

$$c_{03} = g - hu_w \quad (6b)$$

The values for the coefficients in these relationships are given in Table 1 (Cox & Munk 1954).

Table 1. Parameters in slope probability density distribution published by Cox & Munk (1954) (all quantities have to be multiplied by 10^{-3}).

Parameter	Symbol	Clean surface	Slick surface
Upwind coefficients	a	0.0	5.0
	b	3.16	0.78
Crosswind coefficients	c	3.0	3.0
	d	1.92	0.84
Skewness coefficients	e	10.0	0.0
	f	8.6	0.0
	g	40.0	20.0
	h	33.0	0.0
Peakedness coefficients	c_{40}	400.0	360.0
	c_{22}	120.0	100.0
	c_{04}	230.0	260.0

Rewriting ζ_x , ζ_y , σ_u^2 , σ_c^2 , and θ as sums of a constant equilibrium term and a time-dependent perturbation term, respectively, yields

$$\zeta_x = \zeta_{x_0} + \delta\zeta_x \quad (7a)$$

$$\zeta_y = \zeta_{y_0} + \delta\zeta_y \quad (7b)$$

$$\sigma_u^2 = \sigma_{u_0}^2 + \delta\sigma_u^2 \quad (8a)$$

$$\sigma_c^2 = \sigma_{c_0}^2 + \delta\sigma_c^2 \quad (8b)$$

and

$$\theta = \theta_0 + \delta\theta \quad (9)$$

The incidence angle for a plane sea surface θ_0 in expressions (1) and (9), respectively, is now redefined as the effective incidence angle θ_0 for a real sea surface with roughness

$$\theta_0 = \theta_{\text{plane}} + \theta_{\text{rough}} \quad (10)$$

where θ_{plane} is the incidence angle for a plane surface. The tangent square of the incidence angle of the background rough sea surface as a function of u_w has been derived by Cox & Munk (1954) as

$$\tan^2\theta_{\text{rough}} = s_0^2 = \langle \zeta_{x_0}^2 \rangle + \langle \zeta_{y_0}^2 \rangle = 0.003 + 0.0051u_w \pm 0.004 \quad (11)$$

The local normalized upwind and crosswind slope are defined by

$$s_u^2 = \frac{(\zeta_{x_0}^2 + \delta\zeta_x^2)}{(\sigma_{u_0}^2 + \delta\sigma_u^2)} \quad (12a)$$

and

$$s_c^2 = \frac{(\zeta_{y_0}^2 + \delta\zeta_y^2)}{(\sigma_{c_0}^2 + \delta\sigma_c^2)} \quad (12b)$$

where

$$\zeta_{x_0} = -\tan\theta_0 \cos\varphi \quad (13a)$$

and

$$\zeta_{y_0} = -\tan\theta_0 \sin\varphi \quad (13b)$$

with the angle φ between the radar range direction and the upwind direction and

$$\delta\zeta_x = -\tan\delta\theta \cos\varphi \quad (14a)$$

and

$$\delta\zeta_y = -\tan\delta\theta \sin\varphi \quad (14b)$$

Assuming that the time-dependent perturbation terms in relations (7)-(9) caused by the disturbance of the surface current $\delta U(\mathbf{x})$ due to marine sand waves obey also a Gram-Charlier series as defined by expression (3), then the disturbed NRCS $\delta\sigma$ is given by

$$\delta\sigma = \sigma - \sigma_0 = \pi |R(0)|^2 \sec^4(\theta_0 + \delta\theta) \times p(\zeta_{x_0} + \delta\zeta_x, \zeta_{y_0} + \delta\zeta_y) - \sigma_0 \quad (15)$$

where σ is the local NRCS influenced by the disturbance of $\delta U(\mathbf{x})$.

The local joint-probability density function of slopes is now defined by

$$p(\zeta_{x_0} + \delta\zeta_x, \zeta_{y_0} + \delta\zeta_y) \approx \frac{1}{2\pi\sigma_u\sigma_c} \times \left\{ \exp\left[-\frac{1}{2}(s_u^2 + s_c^2)\right] \right\} \times \left\{ 1 - \left(\frac{1}{2}\right) c_{21}(s_c^2 - 1) - \left(\frac{1}{6}\right) c_{03}(s_u^3 - 3s_u) + \left(\frac{1}{4}\right) c_{22}(s_c^2 - 1)(s_u^2 - 1) + \left(\frac{1}{24}\right) [c_{40}(s_c^4 - 6s_c^2 + 3) + c_{04}(s_u^4 - 6s_u^2 + 3)] \right\} \quad (16)$$

The tangent square of the disturbed incidence angle is derived by

$$\tan^2\delta\theta = +\delta\sigma^2 = \delta\sigma_u^2 + \delta\sigma_c^2, \quad \frac{\partial u_{\text{perp}}}{\partial x_{\text{perp}}} \leq 0 \quad (17a)$$

and

$$-\tan^2\delta\theta = -\delta\sigma^2 = -(\delta\sigma_u^2 + \delta\sigma_c^2), \quad \frac{\partial u_{\text{perp}}}{\partial x_{\text{perp}}} > 0 \quad (17b)$$

with

$$\delta\sigma_u^2 = \int_{k_0}^{k_c} \mathbf{k}^2(\mathbf{x}) \delta F(\mathbf{x}, \mathbf{k}) \cos\alpha \, d\mathbf{k} \quad (18a)$$

and

$$\delta\sigma_c^2 = \int_{k_0}^{k_c} \mathbf{k}^2(\mathbf{x}) \delta F(\mathbf{x}, \mathbf{k}) \sin\alpha \, d\mathbf{k} \quad (18b)$$

where x_{perp} is the space variable defined perpendicular to the sand wave crest, \mathbf{k} is the wave number vector of short gravity waves, k_0 is the lower limit of the wave number producing quasi-specular scattering modulation, k_c is the maximum wave number neglecting the effect of surface tension, $\partial u_{\text{perp}} / \partial x_{\text{perp}}$ is the gradient or strain rate of the current velocity perpendicular to the sand wave crest, α is the angle between the upwind direction and the current velocity component perpendicular to the sand wave crest, and $\delta F(\mathbf{x}, \mathbf{k})$ is the perturbation term of the wave-energy density spectrum in the short gravity wave regime caused by wave-current interaction applying weak hydrodynamic interaction theory (Alpers & Hasselmann 1978).

The relationship between $\Psi(\mathbf{k})$, $F(\mathbf{k})$ and the wave action density spectrum $N(\mathbf{k}) = F(\mathbf{k})(\omega'(\mathbf{k}))^{-1}$ is defined by Holliday et al. (1986)

$$F(\mathbf{k}) = \omega'(\mathbf{k})N(\mathbf{k}) = \frac{\omega'(\mathbf{k})^2}{k} \psi(\mathbf{k}) \quad (19)$$

with the wave height spectrum

$$\psi(k) = a_p k^{-4} \quad (20)$$

where a_p is known as the Phillips constant. Based on measurements by Stolte (1990), the empirical relation for a_p as a function of wind speed $u_w \leq 8 \text{ m s}^{-1}$ is used

$$\log_{10} a_p = -2.90 + 3.06 \cdot 10^{-1} u_w - 1.85 \cdot 10^{-2} u_w^2 \quad (21)$$

The dispersion relation for gravity waves in equation (19) is defined by

$$\omega' = (gk)^{1/2} \quad (22)$$

For the modulation of the first order perturbed wave-energy density spectrum $\delta F/F_0 = (F-F_0)/F_0$ (with F_0 as the unperturbed wave-energy density spectrum) the expression derived by Alpers & Hennings (1984) is used

$$\frac{\delta F}{F_0} = -4.5 \frac{\partial u_{\text{perp}}}{\partial x_{\text{perp}}} \left(\left(\mathbf{c}_g + \mathbf{u}_0 \right) \frac{1}{L} + \mu \right)^{-1} \quad (23)$$

with the absolute value of the group velocity for gravity waves

$$|\mathbf{c}_g| = \frac{1}{2} \frac{\omega'}{k} \quad (24)$$

where \mathbf{u}_0 is the mean current velocity of the undisturbed sea area, μ is the relaxation rate parameter, g is the acceleration of gravity, $L = L_{SSL}$ is the length scale of the steep slope, and $L = L_{GSL}$ is the length scale of the gentle slope of the sand wave, respectively.

More information of the weak hydrodynamic interaction theory for the radar imaging mechanism of the sea bed is given in Alpers & Hennings (1984) and Hennings & Herbers (2006). The improved quasi-specular scattering theory as outlined above will be applied and tested for the TerraSAR-X incidence angle of 55° with regard to explain the NRCS modulation caused by marine sand waves. Simulations of the NRCS modulation due to quasi-specular scattering caused by marine sand waves will be carried out as a function of radar incidence angle, radar look direction, tidal current speed and -direction, and wind speed and -direction, respectively. The simulations will be analysed and compared with satellite-borne TerraSAR-X data.

3. TERRASAR-X HIGH RESOLUTION SPOTLIGHT MODE

TerraSAR-X is Germany's first civil national remote sensing satellite realized by a public-private partnership between the German Aerospace Center (DLR) and the European Aeronautic Defence and Space Company (EADS) Astrium GmbH. The radar remote sensing satellite has been launched successfully at 0214 UT 15 June 2007 on a Russian/Ukrainian DNEPR-1 launch vehicle from the Baikonur cosmodrome in Kazakhstan. An artists view of TerraSAR-X is shown in Figure 1. TerraSAR-X is an X-band SAR based on active phased array antenna technology using a radar frequency of 9.65 GHz and a radar wavelength of 3.11 cm. Each pulse can be transmitted either vertically (V) or horizontally (H) polarised. The backscattered signal can be received with either vertical or horizontal polarisation, independent of the transmit polarisation. Imaging will be possible in single, dual, and quad polarisation (on experimental basis). A very high spatial resolution in the flight or azimuth direction can be achieved, if the radar antenna length is short or a spotlight mode is used from the view of sensor technology. Shorter antennas must be larger in the vertical dimension to illuminate the required area, which usually means scanning in elevation to obtain a reasonable swath width. TerraSAR-X is a highly programmable X-band SAR and in the following, a brief description of the innovative spotlight mode sensor technology will be given. The TerraSAR-X spotlight mode allows a very high spatial resolution in azimuth direction. It is based on electrical beam steering in azimuth direction in a way that the same target region is

illuminated during the whole data recording period. In this way the illumination time will be increased,

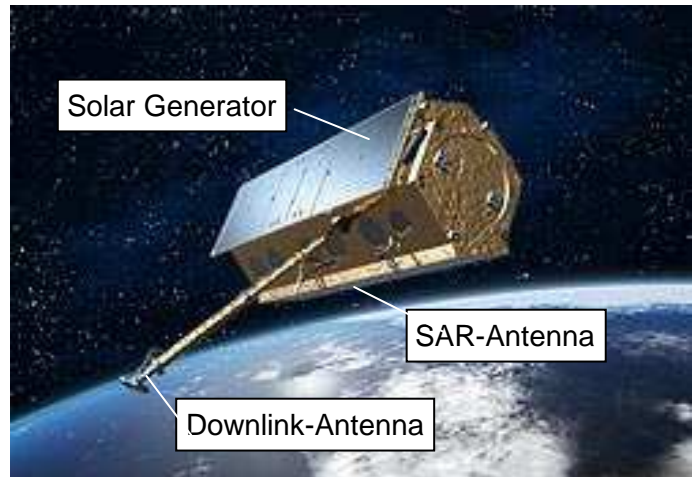


Figure 1. Artists view of TerraSAR-X (modified source: German Aerospace Center (DLR)).

the nominal ground velocity of the radar beam is reduced, the size of the synthetic aperture will become larger and with it a high spatial resolution is achieved. Unfortunately, the larger aperture of a high spatial azimuth resolution results at the expense of azimuthal scene size. The TerraSAR-X sensor technology offers high flexibility in order to image the sea area of interest. A number of 123 spotlight elevation beams are defined in order to adjust the scene center in small increments so that the required area can be placed in the middle of a scene. In azimuth direction about 125 beams from a set of 249 beams are used to extend the synthetic aperture.

The imaging process is started and controlled by the Global Positioning System (GPS). This procedure will be activated when TerraSAR-X reaches a position along the orbit that has been calculated from the required scene center coordinates of the investigated sea area. The TerraSAR-X high resolution spotlight mode (HS) is designed for an azimuth resolution of 1 m resulting in an azimuth scene size of at least 5 km. The characteristic values are given in Table 2.

Table 2. Parameters of TerraSAR-X high resolution spotlight mode.

Parameter	Value
Scene extension	5 km (azimuth) × 10 km (ground range)
Full performance incidence angle range	20° – 55°
Data access incidence angle range	15° – 60°
Number of elevation	95 (full performance)

beams	123 (data access)
Number of azimuth beams	ca. 249
Azimuth steering angle	± 0.75°
Azimuth resolution	1 m (single polarization) 2 m (dual polarization)
Ground range resolution	1.34 m - 3.21 m (at 55° ... 20° incidence angle)
Polarizations	HH or VV (single) HH / VV (dual)

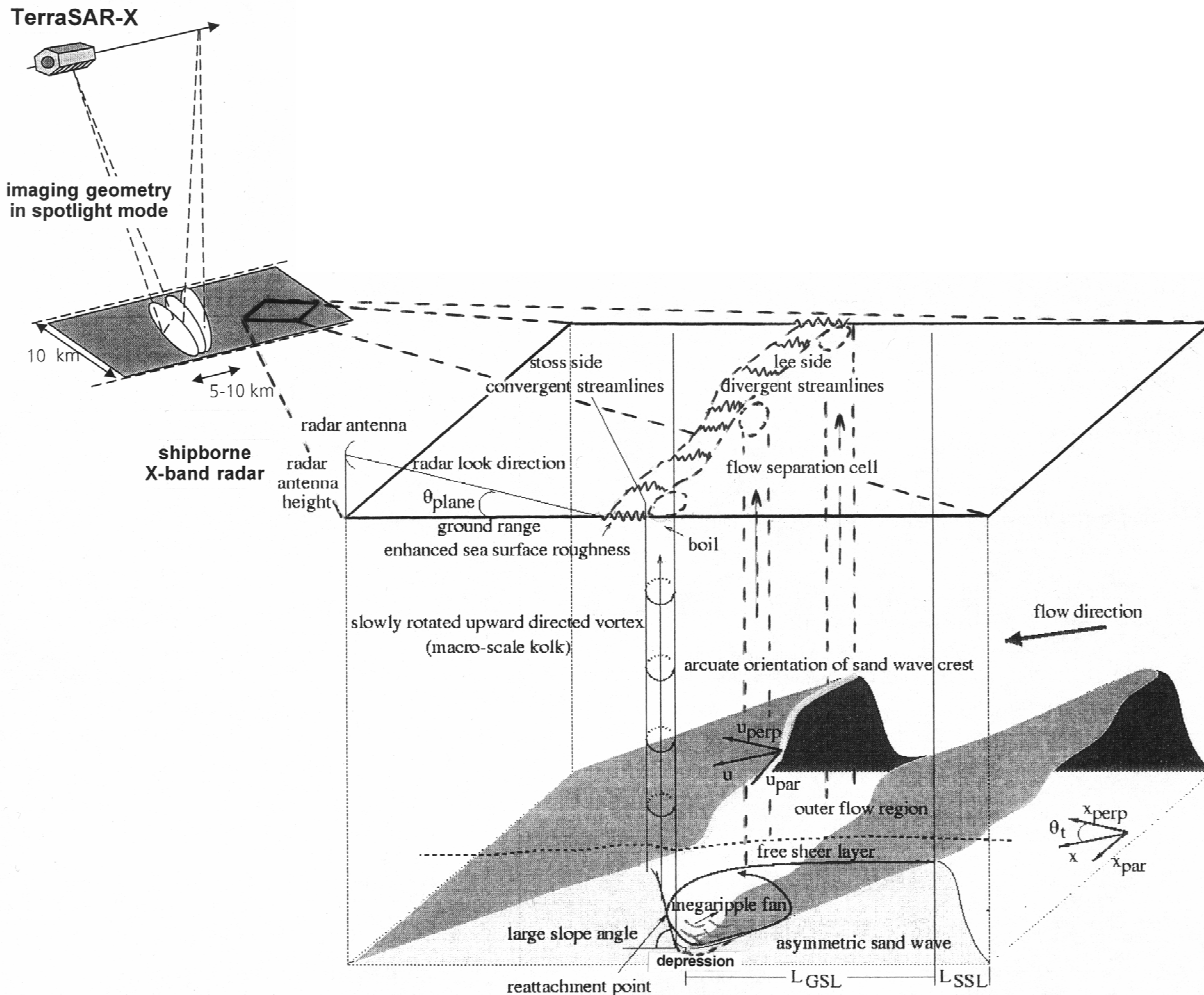


Figure 2. Proposed measurement configuration, TerraSAR-X imaging geometry in spotlight mode, and a schematic sketch of the characteristic fluid flow in the water column, the macroturbulence mechanism caused by ebb tidal currents over flood tide oriented marine sand waves, as well as coordinate systems and definition of symbols defined for the investigations which will be carried out.

Figure 2 shows the proposed measurement configuration, the TerraSAR-X imaging geometry in spotlight mode, and a schematic sketch of the characteristic fluid flow in the water column, as well as the macroturbulence mechanism caused by ebb tidal currents over flood tide oriented marine sand waves.

4. STUDY AREA

The proposed study area is the Lister Tief of the German Bight in the North Sea located north of the island of Sylt. This tidal channel is an ideal test site because of large morphological changes of the sea

bed due to strong tidal current velocities. Therefore, the sea area is of permanent interest for coastal zone management. Within an area of only 6 km² a complex configuration of different bedforms is found. The sand waves investigated in this area are four-dimensional in space and time and have heights ≤ 11 m and widths ≤ 300 m. The migration rate of sand waves can come up to 80 m per year. Small-scale ripples as well as megaripples of widths ≤ 20 m are superimposed on the larger-scale sand waves. Measurements of the lateral distribution of the water transport during two tidal cycles across the inlet of the Lister Tief showed that a net water outflow from the tidal bight can be observed in the

northern part of the analysed cross-section, whereas a net inflow from the open sea is observed in the southern section (Kappenberg et al. 1998). This water transport mechanism is in agreement with observed marine asymmetric sand waves. Flood-tide oriented sand waves are observed in the southern part of the Lister Tief and ebb-tide oriented sand waves are located in the northern part, respectively. Similar results to the water transport described above have been measured for the suspended matter concentration (SPM) which shows an export of SPM in the main channel and in the northern part and an import in the southern part.

In the Lister Tief the interaction of sea bottom topography, current velocity and sea surface can locally be described by the so called kolk-boil mechanism. A strong kolk is a slowly rotating, upward-tilting vortex on the stoss face of a submarine bedform. It may reach the water surface, can create a cloudy columnar sediment-fluid mixture, and form a raised circular or oval patch at the air-water interface, referred to as a boil. These boils have horizontal scales between 5 m and 25 m in the Lister Tief and are comparable to the flow depth itself as a first approximation. The kolk-boil mechanism is visualized by local and space dependent wave steepening at the sea surface. The vortices are manifestations of waterspouts which are the upward orientated components u_{vert} of the three-dimensional current velocity field measured at the stoss faces of asymmetric marine sand waves (Hennings & Herbers 2006). Until now, only two-dimensional profiles of the current velocity as a function of water depth have been analysed in the Lister Tief.

Time, radiometric, and spatial resolution of available spaceborne imaging radars of ERS-1/2, RADARSAT, and ENVISAT ASAR have been considered as too low to investigate radar signatures in detail based on the scales described above and associated with meso-scale processes. To map also the transport characteristics of these bedforms, satellite-borne radar imaging systems of up to 1 m spatial and up to 1.5 dB radiometric resolution, respectively, are needed. TerraSAR-X will satisfy these requirements. With a scene area of 5 km in azimuth and 10 km in ground range direction the whole tidal channel of the Lister Tief will be imaged during one overflight. For the first time, it is expected, that the upward orientated vortex cells manifesting as boils at the water surface can be detected from space relative to the orientation of sand wave crests.

5. CONCLUSIONS

The main objective introduced in this paper is an improved radar imaging theory based on quasi-specular scattering which has to be tested by simulations of the NRCS modulation of marine sand waves

and has to be compared with measured NRCS modulation data acquired by TerraSAR-X. It is assumed that quasi-specular scattering becomes dominant at X-band and higher radar frequencies. This implies that the NRCS for small water surface waves is not proportional to the wave height spectral density at the Bragg backscatter wavenumbers but is proportional to the total variance of slopes created by ocean surface waves. The additional dependences on the up- and crosswind wave slopes, the angle between the upwind and perpendicular current direction to the sand wave crest, and the angle between the radar range direction and the upwind direction are included in the theory. The relaxation rate μ is one of the most crucial parameters in weak hydrodynamic interaction theory and has to be taken into consideration applying the presented theory. Comprehensive discussions concerning μ have been published by Caponi et al. (1988) and Hennings et al. (2001). It has also to be noticed here that the time-dependent perturbation terms caused by the disturbance of the surface current $\delta U(\mathbf{x})$ due to wavy perturbations at the sea bed such as sand waves obey also a Gram-Charlier series which has not to be verified until now.

A high potential in the scientific evaluation of TerraSAR-X data especially for coastal waters is expected based on the very high geometric and radiometric resolution of TerraSAR-X. Very detailed analysis of sea bottom topography signatures at the water surface is feasible. For the first time, it will be possible from space to identify NRCS modulations caused by meso-scale sand waves ≤ 300 m widths at water depths ≤ 40 m. Often, unique oceanographic phenomena such as up- and downwelling events, turbulence, and eddies are associated with marine sand waves in tidal channels. Calhoun & Street (2001) and Calhoun et al. (2001) showed that important dynamical features of turbulent flow over wavy topography can be revealed by studying the instantaneous flow fields. Their conclusion is that Görtler instability (Görtler 1941) appears to be important in the formation of the vortices in their analysed flow over wavy boundaries. Görtler instability is an inviscid instability mechanism occurring in boundary layers over concave surfaces which may cause streamwise oriented vortices. The interaction of hydro-, sediment- and morphodynamics in tidal channels covered by four-dimensional bedforms in time and space is not well understood and has to be improved by using TerraSAR-X data. The proposed research offers good potentials to apply radar remote sensing techniques to coastal zone management and rapid synoptic surveying.

REFERENCES

- Alpers, W. & Hasselmann, K. 1978. The two-frequency microwave technique for measuring ocean wave spectra from an airplane or satellite. *Boundary-Layer Meteorology* 13: 215-230.
- Alpers, W. & Hennings, I. 1984. A theory of the imaging mechanism of underwater bottom topography by real and synthetic aperture radar. *Journal of Geophysical Research* 89(C6): 10529-10546.
- Barrick, D. E. 1968. Rough surface scattering based on the specular point theory. *IEEE Transactions on Antennas and Propagation* AP-16: 449-454.
- Calhoun, R. J. & Street, R. L. 2001. Turbulent flow over a wavy surface: Neutral case. *Journal of Geophysical Research* 106(C5): 9277-9293.
- Calhoun, R. J., Street, R. L. & Koseff, J. R. 2001. Turbulent flow over a wavy surface: Stratified case. *Journal of Geophysical Research* 106(C5): 9295-9310.
- Caponi, E. A., Crawford, D. R., Yuen, H. C. & Saffman, P. G. 1988. Modulation of radar backscatter from the ocean by a variable surface current. *Journal of Geophysical Research* 93(C6): 12249-12263.
- Cox, C. & Munk, W. 1954. Measurement of the roughness of the sea surface from photographs of the sun's glitter. *Journal of the Optical Society of America* 44: 838-850.
- Gargett, A., Wells, J., Tejada-Martinez, A. E. & Grosch, C. E. 2004. Langmuir supercells: a mechanism for sediment resuspension and transport in shallow seas. *Science* 306: 1925-1928.
- Görtler, H. 1941. Instabilität laminarer Grenzschichten an konkaven Wänden gegenüber gewissen dreidimensionalen Störungen. *Zeitschrift für Angewandte Mathematik und Mechanik* 21: 250-252.
- Hennings, I., Lurin, B. & Didden, N. 2001. Radar imaging mechanism of the sea bed: Results of the C-STAR experiment in 1996 with special emphasis on the relaxation rate of short waves due to current variations. *Journal of Physical Oceanography* 31: 1807-1827.
- Hennings, I., Herbers, D., Prinz, K. & Ziemer, F. 2004. First results of the OROMA experiment in the Lister Tief of the German Bight in the North Sea. *EARSel eProceedings* 3: 86-104.
- Hennings, I. & Herbers, D. 2006. Radar imaging mechanism of marine sand waves at very low grazing angle illumination caused by unique hydrodynamic interactions. *Journal of Geophysical Research* 111: C10008, doi:10.1029/2005JC003302.
- Holliday, D., St-Cyr, G. & Woods, N. E. 1986. A radar ocean imaging model for a small to moderate incidence angles. *International Journal of Remote Sensing* 7: 1809-1834.
- Inglada, J. & Garello, R. 2002. On rewriting the imaging mechanism of underwater bottom topography by synthetic aperture radar as a Volterra series expansion. *IEEE Journal of Oceanic Engineering* 27: 665-674.
- Kappenberg, J., Fanger, H.-U. & Müller, A. 1998. Currents and suspended particulate matter in tidal channels of the Sylt-Rømø basin. *Senckenbergiana maritima* 29: 93-100.
- Laban, C. 2006. Seabed mapping in the Dutch sector of the North Sea. *Sea Technology* 47(8): 47-51.
- Lamont-Smith, T., Jackson, A. M., Shepherd, P. W. & Hill, R. D. 2005. Low grazing angle radar imaging experiments over the South Falls sandbank. *International Journal of Remote Sensing* 26: 937-966.
- Marghany, M. & Hashim, M. 2006. Three-dimensional reconstruction of bathymetry using C-band TOPSAR data. *Photogrammetrie Fernerkundung Geoinformation* 2006 (6): 469-480.
- Phillips, O. M. 1984. On the response of short ocean wave components at a fixed wavenumber to ocean current variations. *Journal of Physical Oceanography* 14: 1425-1433.
- Romeiser, R. & Alpers, W. 1997. An improved composite surface model for the radar backscattering cross section of the ocean surface. 2. Model response to surface roughness variations and the radar imaging of underwater bottom topography. *Journal of Geophysical Research* 102(C6): 25251-25267.
- Shuchman, R. A., Lyzenga, D. R. & Meadows, G. A. 1985. Synthetic aperture radar imaging of ocean-bottom topography via tidal-currents interactions: theory and observations. *International Journal of Remote Sensing* 6: 1179-1200.
- Stolte, S. 1990. Dynamics of short waves and wave breaking. *Federal Armed Forces Underwater Acoustics and Marine Geophysics Research Institute Kiel, Report 1990-4*: 48 pp.
- Trueblood, K. N., Bürgi, H.-B., Burzlaff, H., Dunitz, J. D., Gramaccioli, C. M., Schulz, H. H., Shmueli, U. & Abrahams, S. C. 1996. Atomic displacement parameter nomenclature. *Acta Crystallographica A* 52: 770-781.
- Valenzuela, G. R. 1978. Theories for the interaction of electromagnetic and ocean waves-A review. *Boundary-Layer Meteorology* 13: 277-293.
- Van Gastel, K. 1987. Imaging by X band radar of subsurface features: a nonlinear phenomenon. *Journal of Geophysical Research* 92(C6): 11957-11865.
- Vogelzang, J. 1997. Mapping submarine sandwaves with multi-band imaging radar I. Model development and sensitivity analysis. *Journal of Geophysical Research* 102(C6): 1163-1181.
- Zimmerman, J. F. T. 1985. Radar images of the sea bed. *Nature* 314: 224-226.